HHS Public Access

Author manuscript

Cell Rep. Author manuscript; available in PMC 2023 May 31.

Published in final edited form as:

Cell Rep. 2021 January 05; 34(1): 108594. doi:10.1016/j.celrep.2020.108594.

ARHGEF3 Regulates Skeletal Muscle Regeneration and Strength through Autophagy

Jae-Sung You[1,*], **Nilmani Singh**[1], **Adriana Reyes-Ordonez**[1], **Nidhi Khanna**[1,2], **Zehua Bao**[3,4], **Huimin Zhao**[3], **Jie Chen**[1,5,*]

[1]Department of Cell and Developmental Biology, University of Illinois at Urbana-Champaign, Urbana, IL 61801, USA

[2]Modalis Therapeutics, Cambridge, MA 02138, USA

[3]Department of Chemical and Biomolecular Engineering and Carl R. Woese Institute for Genomic Biology, University of Illinois at Urbana-Champaign, Urbana, IL 61801, USA

[4]Department of Biomedical Engineering and Biological Design Center, Boston University, Boston, MA 02215, USA

[5]Lead Contact

SUMMARY

Skeletal muscle regeneration after injury is essential for maintaining muscle function throughout aging. ARHGEF3, a RhoA/B-specific GEF, negatively regulates myoblast differentiation through Akt signaling independently of its GEF activity *in vitro*. Here, we report ARHGEF3's role in skeletal muscle regeneration revealed by ARHGEF3-KO mice. These mice exhibit indiscernible phenotype under basal conditions. Upon acute injury, however, ARHGEF3 deficiency enhances the mass/fiber size and function of regenerating muscles in both young and regeneration-defective middle-aged mice. Surprisingly, these effects occur independently of Akt but via the GEF activity of ARHGEF3. Consistently, overexpression of ARHGEF3 inhibits muscle regeneration in a Rho-associated kinase-dependent manner. We further show that ARHGEF3 KO promotes muscle regeneration through activation of autophagy, a process that is also critical for maintaining muscle strength. Accordingly, ARHGEF3 depletion in old mice prevents muscle weakness by restoring autophagy. Taken together, our findings identify a link between ARHGEF3 and autophagy-related muscle pathophysiology.

Graphical Abstract

*Correspondence: youj@illinois.edu (J.-S.Y.), jiechen@illinois.edu (J.C.).

AUTHOR CONTRIBUTIONS

J.-S.Y. and J.C. designed the study. Z.B. and H.Z. designed and created the TALENs. N.S., A.R.-O., N.K., and J.-S.Y. generated mouse lines. J.-S.Y. acquired and analyzed data. J.-S.Y. and J.C. wrote the manuscript. N.S., N.K., and H.Z. edited the manuscript.

SUPPLEMENTAL INFORMATION

Supplemental Information can be found online at https://doi.org/10.1016/j.celrep.2020.108594.

DECLARATION OF INTERESTS

The authors declare no competing interests.

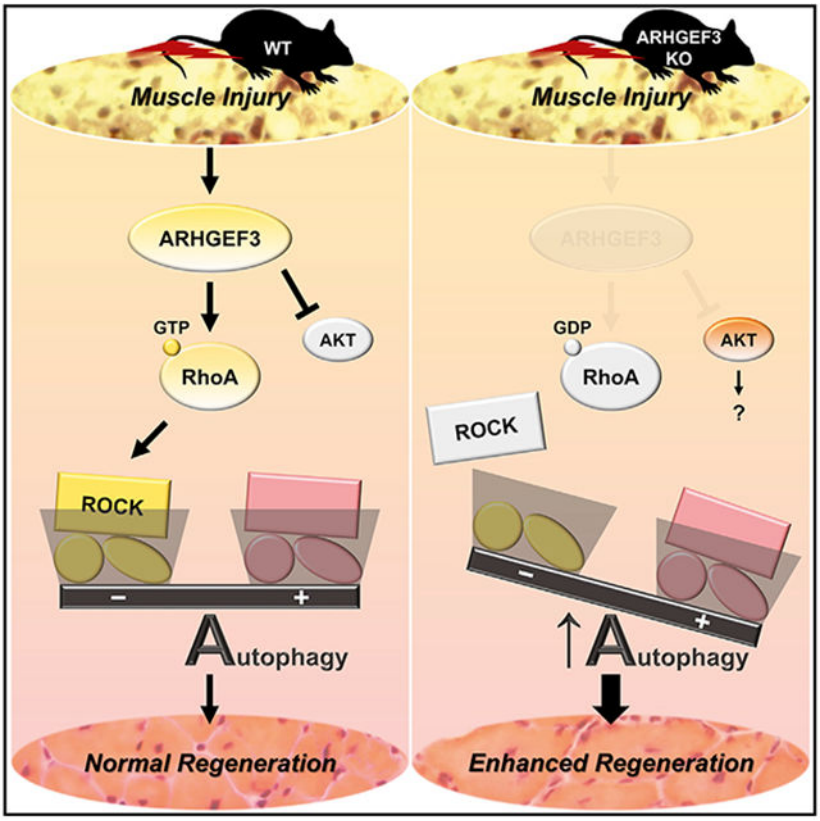

In Brief

Post-injury regeneration and aging significantly affect skeletal muscle function. One of the mechanisms governing these processes is autophagy. You et al. identify ARHGEF3 as an endogenous inhibitor of autophagy in muscles after injury as well as during aging. Through autophagy, ARHGEF3 deficiency enhances muscle regeneration and prevents age-related muscle weakness.

INTRODUCTION

Skeletal muscle possesses robust regeneration capacity that is essential for restoration of intact muscle function upon injury. Skeletal muscle regeneration requires a highly coordinated myogenesis process consisted of muscle stem cell proliferation, cell-cycle exit, and differentiation and fusion of mono-nucleated myoblasts, as well as timely modulation of these processes by cell-intrinsic and cell-extrinsic (e.g., immune cells, cytokines) factors (Le Grand and Rudnicki, 2007; Tidball, 2017). Although many intrinsic signaling molecules regulating these processes have been identified *in vitro*, their role in muscle regeneration *in vivo* is still largely unexplored. Nevertheless, some intracellular mechanisms critical for muscle regeneration have recently been identified. For example, autophagy, a key homeostatic process necessary for degradation of unwanted cellular components, plays a crucial role in successful muscle regeneration after injury (Call et al., 2017; García-Prat et

al., 2016; Paolini et al., 2018). Again, however, molecules that regulate autophagy during regeneration are poorly understood.

More than 10 years ago, many research groups were interested in and investigated the role of RhoA-Rho-associated kinase (ROCK) signaling in myogenic differentiation, and they came to the conclusion that RhoA-ROCK regulation of myogenesis in cells is cell-stage-specific: it is necessary for myoblast proliferation and maintenance of myogenic capacity, but it suppresses differentiation once cells exit the cell cycle and enter the post-proliferative phase (Charrasse et al., 2006; Iwasaki et al., 2008; Lim et al., 2007; Takano et al., 1998; Wei et al., 1998). Although these studies suggested the potential involvement of a guanine nucleotide exchange factor for Rho GTPases (Rho-GEF) in skeletal muscle regeneration, there has been no report of a role of any endogenous RhoGEF (among ~70 in the human genome; Rossman et al., 2005) in muscle regeneration. Perhaps targeting RhoA-ROCK signaling with such complex and paradoxical effects is presumed to be less clinically feasible and effective.

Since then, Khanna and colleagues have examined ARHGEF3 (also called XPLN), which selectively activates RhoA and RhoB (Arthur et al., 2002), and found that this RhoGEF negatively regulates myoblast differentiation through inhibition of the mammalian target of rapamycin complex 2 (mTORC2) activation of Akt (Khanna et al., 2013), one of the best established myogenic factors (Jiang et al., 1999). Interestingly, in that study, ARHGEF3 exerted these functions independently of its GEF activity, thus raising the possibility that ARHGEF3 could become a mechanistically feasible target for regulating skeletal muscle regeneration regardless of its role in RhoA/B signaling. In the present study, we investigated this possibility by creating ARHGEF3-knockout (KO) mice. These mice showed no discernible phenotype under basal conditions. However, depletion of ARHGEF3 promoted injury-induced muscle regeneration and strength regain. Unexpectedly, these effects of ARHGEF3 KO did not require activation of Akt signaling, but instead they occurred through a mechanism involving the GEF activity of ARHGEF3 and autophagy.

RESULTS

ARHGEF3 KO Promotes Skeletal Muscle Regeneration after Injury

Arhgef3 gene-edited mice were created by using TALENs (Sun and Zhao, 2013) that target exon 3, the earliest region shared by all four established *Arhgef3* transcript variants, in the germline. A mouse line containing a 17 bp deletion in exon 3 (thus causing open reading frameshift) was selected for further characterization. Mice were bred to yield homozygous mutant offspring, identified by genotyping with three independent PCR-based methods (Figure 1A). As expected, muscles from the mutant mice expressed a reduced level of *Arhgef3* transcripts (Figure 1B, left panel) most likely because of nonsense-mediated RNA decay. Furthermore, sequencing of the remaining transcripts confirmed the frameshift deletion of exon 3 and introduction of premature stop codons (Figure 1B, right panel; Figure S1A). Only a small portion of the N terminus of ARHGEF3 would be translated from this mutant mRNA, which is unlikely to result in a functional or even stable protein. From here on, we refer to the homozygous mutant mice as ARHGEF3 KO. These mice, at their young (3 months) and mature (6 months) adult ages, did not exhibit any discernible phenotype under normal conditions on the basis of body composition (Figure 1C), muscle mass and

force, fatigability, and injury susceptibility (Figures S1B-S1E). Other muscle properties, including expression of myosin heavy chain isoforms (i.e., fiber types), mitochondrial proteins (COX IV and cytochrome *c*), and muscle stem cell and macrophage markers (*Pax7* and *F4/80*, respectively), were also indistinguishable between WT and ARHGEF3-KO mice (Figures S1F and S1G).

To address the role of ARHGEF3 in skeletal muscle regeneration, tibialis anteria (TA) muscles from wild-type (WT) and ARHGEF3-KO mice were injected with $BaCl_2$, which induces muscle fiber necrosis and subsequent regeneration. Upon injury, the ARHGEF3 protein was transiently elevated in WT, but not in ARHGEF3-KO, muscles (Figure 2A), allowing its detection by western blotting and further confirmation of ARHGEF3 KO. Detection of ARHGEF3 by western blotting has been a long-standing challenge. We tested nearly all commercially available antibodies, and none was validated in cells by ARHGEF3 knockdown. Our custom-made antibody used here was the only one validated (Khanna et al., 2013), although its avidity is not high.

Over the course of regeneration, muscle mass increased steadily in WT mice, as expected, and this increase was further enhanced in both male and female ARHGEF3-KO mice (Figure 2B), suggesting that KO of ARHGEF3 promoted muscle regeneration. To further assess regeneration, we analyzed cross-sectional area of the newly regenerating myofibers identified by their central nuclei (Figure 2C) and found that KO of ARHGEF3 led to a shift of regenerating myofibers to larger sizes, resulting in a significant increase in the average size (Figure 2D).

Next, we asked whether those morphological effects of ARHGEF3 KO were functionally relevant. To address that, we measured muscle force over the course of regeneration. Similar to muscle mass changes, total muscle force progressively increased after injury and ARHGEF3 KO further enhanced the force in both male and female mice (Figures 2E and 2F). These results clearly demonstrate that depletion of the ARHGEF3 protein promotes skeletal muscle regeneration *in vivo*. It is also noteworthy that in female mice, this ARHGEF3 KO-promoted recovery of muscle mass and force occurred at an earlier time point after injury (7 days) than in male mice, suggesting a potential sexual dimorphism by ARHGEF3 in the early phase of muscle regeneration. Nevertheless, the overall phenotype was consistent between male and female mice, and thus we pursued next experiments with one gender, whichever available.

ARHGEF3 Regulation of Muscle Regeneration Is Independent of Its Effect on Akt Signaling

Next, we wanted to determine the mechanism underlying the effects of ARHGEF3 KO on muscle regeneration. Previously, it had been shown that knockdown of ARHGEF3 increases myogenic mTORC2-Akt signaling in C2C12 myoblasts (Khanna et al., 2013). To investigate the involvement of mTORC2-Akt signaling, we examined phosphorylation status of mTORC2 substrates, including Ser473-Akt, Ser657-PKCα (Ikenoue et al., 2008), and SGK1 (Garcéa-Martínez and Alessi, 2008), in injured regenerating muscles. As shown in Figures 3A and S2, ARHGEF3 KO increased phosphorylation of Ser473-Akt but not Thr308-Akt, Ser657-PKCα, or Thr346-NDRG1 (a substrate of SGK1). These observations

are consistent with the previous *in vitro* finding that ARHGEF3 specifically inhibits mTORC2 phosphorylation of Akt (Khanna et al., 2013).

To directly test whether the effects of ARHGEF3 KO on muscle regeneration is mediated by the increased phosphorylation of Akt, we treated mice with the Akt inhibitor triciribine. Its metabolite triciribine phosphate blocks membrane recruitment and subsequent phosphorylation of Akt without affecting its kinase domain (Berndt et al., 2010), thus inhibiting hyper-activation of Akt under stimulated conditions (i.e., ARHGEF3 KO) while maintaining basal activity of Akt essential/permissive for myogenesis. As expected, muscles from ARHGEF3-KO mice treated with control vehicle displayed increased muscle mass and force compared with that from WT mice after injury (Figure 3B). Surprisingly, however, triciribine did not prevent any of these effects of ARHGEF3 KO (Figure 3B) despite substantial inhibition of phosphorylation of Akt and its substrate GSK3β (Figure 3C). Hence, we conclude that ARHGEF3 KO promotes muscle regeneration through a mechanism independent of its effect on Akt signaling.

The GEF Activity of ARHGEF3 and ROCK Are Critical for the Regulation of Muscle Regeneration

The observation that ARHGEF3 KO exerted more prominent effects on muscle regeneration after the proliferative stage (0–7 days) (Tidball and Villalta, 2010) in Figure 1 is consistent with the cell-stage-specific role of RhoA-ROCK signaling in myogenesis *in vitro* (Iwasaki et al., 2008). Hence, we considered a potential involvement of the GEF activity of ARHGEF3 in the regulation of muscle regeneration. Indeed, we found that RhoA-specific GEF activity was elevated in injured muscles, and this increase was substantially reduced by ARHGEF3 KO (Figure 4A), which suggests a dominant role of ARHGEF3 in RhoA signaling during regeneration. To probe a functional relevance of the GEF activity, we introduced recombinant ARHGEF3, WT, or a GEF-inactive mutant (L269E) (Khanna et al., 2013) by *in vivo* transfection into ARHGEF3-KO muscles at 10 days post-injury (Figure 4B), a time point after which the muscles undergo the post-proliferative phase of regeneration. Furthermore, at this time point, F4/80-positive infiltrating macrophages, which may complicate the interpretation of our experiments, remarkably subsided (Figure 4B). As shown in Figure 4C, the ARHGEF3-KO muscles transfected with WT-ARHGEF3 displayed higher RhoA GEF activity than that with empty vector or L269E-ARHGEF3, and the differences were similar to that between intact WT and ARHGEF KO regenerating muscles (Figure 4A). Moreover, the difference in RhoA GEF activity between WT- and L269E-ARHGEF3 did not affect Ser473-Akt phosphorylation (Figure 4C), which is consistent with the GEF-independent role of ARHGEF3 on Akt phosphorylation (Khanna et al., 2013). Strikingly, expression of recombinant WT- but not L269E-ARHGEF3 reduced regenerating muscle mass and force in the KO mice, reconstituting the regeneration phenotype of WT muscles (Figure 4D). Collectively, these results not only prove that the loss of ARHGEF3 is responsible for the regeneration phenotype of ARHGEF3-KO mice but also demonstrate that the ARHGEF3-regulated muscle regeneration requires its GEF activity.

To determine whether ROCK, a major downstream effector of RhoGEF/RhoA, mediates ARHGEF3-regulated muscle regeneration, we transfected WT-ARHGEF3 into regenerating

WT muscles and then treated the mice with the ROCK inhibitor Y-27632 (Figure 4E). As shown in Figure 4F, muscles transfected with ARHGEF3 in the absence of Y-27632 exhibited reduced mass and force compared with that with empty vector, further validating that ARHGEF3 negatively regulates muscle regeneration (Figure 4F). Notably, Y-27632 completely prevented these effects of ARHGEF3 overexpression (Figure 4F). These results suggest ROCK as an essential mediator of the ARHGEF3-regulated muscle regeneration and further corroborate the critical role of ARHGEF3's GEF activity in muscle regeneration.

ARHGEF3 KO Does Not Affect the Expression of Inflammatory Markers in Regenerating Muscles

A coordinated inflammatory response to injury plays a central role in the progress of muscle regeneration (Tidball, 2017). Our data showed that ARHGEF3 KO in male mice did not affect regeneration at an early time point after injury (7 days) but promoted regeneration at later time points. It is widely agreed that at 7 days post-injury, most of the initial pro-inflammatory responses have switched to an anti-inflammatory environment that supports muscle differentiation and growth (Tidball, 2017). It is possible that depletion of ARHGEF3 in immune cells may have influenced the anti-inflammatory environment around the early time point and subsequently enhanced the later phase of muscle regeneration. Hence, we examined mRNA levels of several anti-inflammatory markers (*Il-10, Il-4, Mrc1*) as well as pro-inflammatory markers (*Ifng, Tnf, Nos2*) at 7 days after injury. The results showed that none of those markers were significantly altered by ARHGEF3 KO in either male or female mice (Figure S3). Although the role of non-muscle cells still cannot be ruled out, these observations combined with the results from the ectopic expression of ARHGEF3 (Figure 4) suggest that the regulation of muscle regeneration by ARHGEF3 KO is driven mainly by muscle cells or muscle stem cells.

ARHGEF3 KO Promotes Muscle Regeneration through Autophagy and Prevents Age-Related Regenerative Defects

It has previously been reported that ROCK negatively regulates autophagy flux under amino acid starvation *in vitro* (Mleczak et al., 2013). This link between ROCK signaling and autophagy has recently been further supported by the use of ROCK KO mice: deletion of ROCK1 restored autophagy flux that was impaired by doxorubicin, a broad-spectrum anti-cancer drug, in cardiomyocytes (Shi et al., 2018), and ROCK1/ROCK2 double deletion promoted basal autophagy and reduced cardiac fibrosis during aging (Shi et al., 2019). In light of the pivotal role of ARHGEF3's GEF activity in muscle regeneration and this reported link between ROCK signaling and autophagy, we hypothesized that ARHGEF3 KO might promote autophagy to enhance muscle regeneration.

We first examined autophagy flux during regeneration with the autophagy marker LC3-II, a lipidated form of LC3-I. LC3-II was elevated in muscles injected with $BaCl_2$, and this increase was further augmented by the treatment of the autophagy inhibitor chloroquine; the effect of chloroquine was similar in injured and uninjured control muscles (Figures 5A and S4A). Because the level of LC3-II accumulation by autophagy blockage reflects the level of autophagy flux, these results indicate that autophagy flux was not altered during regeneration. We then compared WT and ARHGEF3-KO muscles and found that the level

of LC3-II was significantly reduced by ARHGEF3 KO in injured muscles (Figures 5B and S4B, left panels). To determine whether this reduction was due to increased autophagic degradation of LC3-II or decreased conversion of LC3-I into LC3-II, we also compared injured muscles from WT and ARHGEF3 KO after chloroquine treatment and found no difference in the level of LC3-II (Figures 5B and S2B, right panels). Hence, these results indicate that ARHGEF3 KO increased autophagy flux and thus the autophagic degradation of LC3-II after injury. In support of this notion, ARHGEF3 KO also reduced the protein level of another autophagy-selective substrate p62 in injured muscles without affecting its mRNA levels (i.e., increased autophagic degradation of p62) (Figures 5C and 5D).

We next asked if this increase in autophagy flux by ARHGEF3 KO was responsible for the enhanced muscle regeneration in ARHGEF3-KO muscles. As shown in Figure 5E, inhibition of autophagy by chloroquine abolished the ARHGEF3 KO-induced increases in muscle mass and force after injury. Therefore, it is highly likely that ARHGEF3 KO promotes muscle regeneration by enhancing autophagy after injury.

Skeletal muscle regenerative capacity declines with aging because of a suppression of autophagy in multiple cell types (Lee et al., 2019). Hence, we envisioned that ARHGEF3 KO with autophagy-promoting effect would counteract the age-related decline in muscle regenerative capacity. As shown in Figure 5F, the recovery of muscle mass and total muscle force after injury was clearly retarded in 10-month-old mice compared with 3-month-old mice. These age-related regenerative defects were not associated with any change in ARHGEF3 levels (Figure S4C). Importantly, however, ARHGEF3 KO significantly improved muscle regeneration in the older mice (Figure 5F). Furthermore, 3-methyladenine (3-MA), which inhibits autophagy via the class III phosphatidylinositol 3-kinase, abrogated the ARHGEF3 KO-promoted muscle regeneration (Figure 5F). We also found that, unlike in young animals (Figures 2B and 2E), the effects of ARHGEF3 KO in 10-month-old mice appeared particularly prominent in total muscle force compared with that in muscle mass (Figure 5F) and that this was due to a robust recovery of muscle-specific force (i.e., muscle quality) that was also entirely 3-MA dependent (Figure 5G). Together, these results suggest that ARHGEF3 is a potential target for preventing autophagy-dependent loss of regenerative capacity during aging.

ARHGEF3 KO Prevents Age-Related Muscle Weakness by Restoring Autophagy Flux

The effect of ARHGEF3 KO on regenerating muscle quality in the middle-aged mice (Figure 5G) is particularly interesting because, even in the absence of injury, skeletal muscle undergoes a loss of muscle strength with aging (dynapenia), and this occurs to a much greater degree than age-related loss of muscle mass (sarcopenia) (Goodpaster et al., 2006; Metter et al., 1999; Russ et al., 2012). An emerging body of evidence also strongly suggests that this age-related loss of specific muscle strength, or muscle quality, is attributable to a decline in basal autophagy and subsequent defects in force transmission apparatus including neuromuscular junction (Bujak et al., 2015; Carnio et al., 2014; Demontis and Perrimon, 2010; Sebastián et al., 2016). Hence, it is plausible to consider a link among ARHGEF3, autophagy, and muscle quality in aging.

To further establish a link between autophagy and muscle quality, we performed an experiment in which young mice received a single dose of chloroquine for time-course examination of muscle quality. As shown in Figure 6A, chloroquine rapidly induced a transient loss of specific muscle force, and its temporal pattern was in a close inverse relationship with the level of LC3-II accumulation, as well as the twitch/tetanic force ratio representing innervation ratio (Celichowski and Grottel, 1993). Of note, the innervation ratio increases with aging (Brooks and Faulkner, 1988; Fling et al., 2009; Kung et al., 2014).

Then, we went on to address whether ARHGEF3 KO could preserve muscle quality in old mice by modulating autophagy. Compared with fully grown 6-month-old adult mice, 18-month-old WT mice did not show any evidence of age-related muscle loss, as previously reported (Hamrick et al., 2006), and nor did ARHGEF3-KO mice (Figure 6B). However, specific muscle force was significantly diminished by aging in WT mice and this decline in muscle quality was completely prevented in ARHGEF3-KO mice (Figure 6C). We also found that ARHGEF3 KO reduced aging-induced accumulation of LC3-II and p62 (Figure 6D). Unlike in young mice, a single dose of chloroquine did not further decrease specific muscle force or increase LC3-II level in old WT mice, confirming that these mice were already suffering from severe autophagy inhibition (Figures 6C and 6D). However, in old ARHGEF3-KO mice, chloroquine both decreased specific muscle force and increased the level of LC3-II, leading to a complete reversal of the rescue effects of ARHGEF3 KO on aging-induced deterioration in muscle quality and basal autophagy (Figures 6C and 6D). The same pattern of changes was also observed in twitch/tetanic force ratio (Figure 6E). Overall, these results demonstrate that depletion of ARHGEF3 allows maintenance of basal autophagy flux and thereby preserves muscle quality in aging muscle.

DISCUSSION

Skeletal muscle's ability to regenerate has an immediate clinical relevance in pathological and non-pathological conditions such as muscular dystrophies, post-injury recovery, and aging. In this study, by using TALEN-mediated gene editing, we demonstrated that depletion of ARHGEF3 promoted functional muscle regeneration after injury and that its GEF activity was necessary for the inhibitory effects of ARHGEF3. We also found that depletion of ARHGEF3 rescued specific muscle strength in old mice and that all these effects were driven by autophagy activation. Hence, our findings uncover ARHGEF3 as a regulator of muscle regeneration and muscle quality and highlight ARHGEF3 as a potential therapeutic target for impaired muscle regeneration and function as well as other clinical issues that result from autophagy defects (Levine and Kroemer, 2008).

On the basis of the present knowledge derived from *in vitro* studies, endogenous ARHGEF3 exerts two molecular functions, one as a RhoGEF toward RhoA/B and the other as an inhibitor of mTORC2-Akt signaling (Arthur et al., 2002; Khanna et al., 2013). In agreement with those activities, we have found that ARHGEF3 KO resulted in reduced RhoA GEF activity and increased mTORC2-Akt signaling in regenerating mouse skeletal muscle, which were reversed by ectopic replenishment of ARHGEF3. Hence, we examined involvement of both mechanisms and found that RhoGEF activity and its downstream effector ROCK, rather than the well-established myogenic mTORC2-Akt signaling, mediate the negative

regulation of muscle regeneration by ARHGEF3. Furthermore, our findings implicated autophagy in the pathway through which ARHGEF3-RhoA/B-ROCK signaling regulates muscle regeneration. This mechanism is consistent with the previous reports that genetic or pharmacological inhibition of ROCK induced rapid formation of enlarged autophagosomes (Mleczak et al., 2013) and autophagy activation (Mleczak et al., 2013; Shi et al., 2018, 2019). It will be interesting to investigate whether ARHGEF3 is also involved in other muscular pathophysiology regulated by RhoA/B-ROCK signaling and autophagy, such as muscular dystrophies (Fiacco et al., 2016; Mu et al., 2013).

Autophagy is also suppressed by Akt via its multiple downstream effectors, including mTORC1, FoxOs, and Beclin1 (Mammucari et al., 2007; Panzhinskiy et al., 2013; Wang et al., 2012). Because ARHGEF3 both activates RhoA/B upstream of ROCK and inhibits Akt, it is reasonable to propose a model in which depletion of AGHGEF3 regulates autophagy by reducing the inhibitory RhoA/B-ROCK signaling while simultaneously suppressing autophagy with Akt activation. Although these two opposing effects of autophagy are expected to counteract each other, our observation of autophagy induction in regenerating muscle with AGHGEF3 depletion indicates that ARHGEF3 acts more predominantly on the RhoA/B-ROCK-autophagy pathway than the Akt-autophagy pathway during regeneration. However, we also speculate that once this Akt-mediated autophagy suppression mode is released by an Akt inhibitor such as triciribine, autophagy would be further activated in ARH-GEF3-KO muscles, offsetting any negative effect the Akt inhibitor may have on myogenesis.

In this study, depletion of ARHGEF3 in mice did not result in any phenotype under basal conditions, but it exerted beneficial effects in the contexts of injury and aging through activation of autophagy. These results suggest that the activity of ARHGEF3 toward autophagy inhibition is switched on only under stressful conditions such as muscle injury or aging. This mode of action may make ARHGEF3 a particularly suitable therapeutic target to allow induction of autophagy specifically in afflicted tissues without the side effects of unnecessary boosting of autophagy in non-targeted or healthy cells/tissues that could disrupt cellular homeostasis (Thorburn, 2018). In order to elaborate therapeutic strategies targeting ARHGEF3, it will be of great importance for future studies to probe how ARHGEF3 activity is regulated under those specific conditions.

STAR★METHODS

RESOURCE AVAILABILITY

Lead Contact—Further information and requests for resources and reagents should be directed to and will be fulfilled by the Lead Contact, Jie Chen (jiechen@illinois.edu).

Material Availability—An *Arhgef3*-KO mouse line generated in this study is available from the Lead Contact.

Data and Cod Availability—This study did not generate/analyze any datasets or code.

EXPERIMENTAL MODEL AND SUBJECT DETAILS

Mice—All animal experiments were performed in accordance with protocols approved by the Institutional Animal Care and Use Committee at the University of Illinois at Urbana-Champaign (#16157 and 19255). WT and *Arhgef3*-KO (detailed in Method details) mouse lines were maintained on a C57BL/6N background and genotyped as described in Figure 1A. All mice were group-housed in cages connected to an EcoFlo ventilation system (Allentown Inc.) in a specific-pathogen-free animal facility kept at 23°C on a 12-hour light/dark cycle and received a pellet diet and water *ad libitum*. Mice from the same pedigree were randomly allocated to the various experimental groups except when they were used for some parameters that required a similar body weight across the groups such as CSA. The animals were anesthetized with isoflurane during all surgical procedures and at the end of the experiments for euthanasia. The sex, age, and number of mice used in each study were specified in the figures or the associated legends, and the influence of sex on the results of the study was described in the Results.

METHOD DETAILS

Generation of ARHGEF3 KO mice—We constructed five pairs of pCS2+TALEN plasmids targeting different regions of exon 3 of the mouse *Arhgef3* gene. Each pair of the plasmids was transfected in C2C12 myoblasts, and genomic DNA was extracted after 3 days of transfection. The genomic region encompassing the TALEN binding sites was PCR-amplified and screened for successful mutations by using the SURVEYOR Mutation Detection Kit (Transgenomic). A TALEN pair selected for *in vivo Arhgef3* editing (see Figure 1A for TALEN binding sites) was linearized with ApaI and transcribed into mRNA using the mMESSAGE mMACHINE SP6 transcription Kit (Invitrogen). The RNA was purified with the MEGAclear Transcription Clean-Up Kit (Invitrogen) and resuspended in T10E0.1 injection buffer. The RNA solution was microinjected into C57BL/6N embryos at the pronuclear stage, and resulting founder (F_0) mice were analyzed by Surveyor assays as described above using tail genomic DNA. Selected founders were further characterized by DNA sequencing of the mutant allele, and mice harboring a 17-base pair deletion in exon 3 of *Arhgef3* were mated to WT mice to obtain heterozygous F_1 progeny.

Body composition Analyses—Longitudinal analyses of body composition including lean and fat weight were performed by scanning mice in an EchoMRI (magnetic resonance imaging)-700 Body Composition Analyzer (EchoMRI).

Muscle injury and drug injections—Muscle injury was induced by injecting 50 μL of 1.2% (w/v) $BaCl_2$ dissolved in saline into TA muscle. As a control, the same volume of saline was injected into the contralateral TA muscle. For systemic drug administration, the following stock solutions were diluted in PBS and injected intraperitoneally into mice at the indicated concentrations: triciribine in DMSO, 1 mg/kg body weight (Yang et al., 2004); Y-27632 in DMSO, 5 mg/kg; chloroquine in deionized water, 50 mg/kg (Fiacco et al., 2016); 3-MA in DMSO, 10 mg/kg (Fiacco et al., 2016). Control mice were injected with an equivalent amount of vehicle diluted in PBS. These injections were repeated every 24 hours after injury unless otherwise indicated.

Skeletal muscle transfection—*In vivo* transfection of TA muscle was performed by electroporation as previously described (You et al., 2018) with slight modifications. Briefly, a small incision was made on the skin covering the distal area of the TA muscle. A 30 μL of plasmid DNA solution containing either pCMV-Myc-ARHGEF3 (Arthur et al., 2002), pCMV-Myc-ARHGEF3-L269E (Khanna et al., 2013), or pcDNA3 empty vector was injected into the distal end of the TA muscle with a 27-gauge needle. After the injection, two stainless steel pin electrodes (1-cm gap) connected to an ECM 830 electroporation unit (BTX/Harvard Apparatus) were laid on top of the muscle, and eight 20-ms square-wave electric pulses were delivered at a frequency of 1 Hz with a field strength of 50 V/cm. After electroporation, the incised skin was closed with a 3-0 polysorb suture.

In situ* muscle force analyses—In situ* force measurement of TA muscle was performed using a 1300A Whole-Animal System (Aurora Scientific). The anesthetized mouse was placed on an isothermal stage set at 38°C, and the skin covering TA muscle and patella was incised. The distal tendon of TA muscle was tied with a 3-0 suture line and cut to isolate the muscle from tibia. After stabilizing the hindlimb by inserting a needle through a fixed post and patella tendon, the suture line was hooked onto the lever arm of the force transducer. Two electrodes were then placed on either side of the TA muscle and electrical stimulations were elicited with 0.2-ms square-wave pulses at 0.2 mA. Once muscle length was adjusted to optimal muscle length where maximal twitch force was produced, maximum isometric tetanic force was determined in the frequency range of 50-200 Hz with 300-ms pulse duration. All tetanic contractions were separated by a 1-minute rest except when muscles were fatigued with one contraction per second for 180 s. For eccentric contractions, TA muscle was lengthened to 1.2 fiber length (0.6 × optimal muscle length) at a velocity of 1.5 fiber length/s and held for 200 ms before being returned to its optimal length at the same velocity. The muscle was stimulated 100 ms prior to and during the lengthening period at 100 Hz. Isometric tetanic force was measured in-between every two eccentric contractions. Throughout the experiments, the exposed TA muscle was kept moist with a warm PBS-soaked KimWipe. Physiological cross-sectional area (pCSA) was calculated by dividing muscle mass by the product of fiber length and muscle density (1.06 g/cm^3). Specific isometric tetanic force was calculated by dividing maximal isometric tetanic force by pCSA.

Histochemical analyses—Isolated TA muscles were submerged in Tissue-Tek OCT compound (Sakura Finetek) at resting length and frozen in liquid nitrogen–chilled isopentane. Mid-belly cross-sections of 10 μm thickness were made with a Microm HM550 cryostat (Thermo Fisher Scientific) at −25°C, placed on microscope slides, and subjected to H&E staining. H&E-stained images randomly chosen were captured with a 20X dry objective (Fluotar, numerical aperture 0.4; Leica) on a Leica DMI 4000B microscope and analyzed for CSA of centrally nucleated regenerating myofibers using ImageJ (NIH). Investigators were blinded to the sample identification during all procedures.

Western blotting—Isolated muscles were immediately frozen in liquid nitrogen and homogenized with a Polytron in ice-cold buffer A containing 50 mM Tris (pH 7.4), 0.5% sodium deoxycholate, 0.1% SDS, 1% Triton X-100, 500 mM NaCl, 10 mM $MgCl_2$, 0.1

mM Na_3VO_4, 25 mM NaF, 25 mM β-glycerolphosphate, and 1 × protease inhibitor cocktail (P8340, Sigma-Aldrich). The homogenates were pre-cleared by centrifugation at 16,200 g for 10 min (4°C). For the detection of F4/80, the frozen muscles were homogenized in ice-cold buffer B containing 20 mM Tris (pH 7.4), 0.3% Triton X-100, 2 mM EGTA, 2 mM EDTA, 0.1 mM Na_3VO_4, 25 mM NaF, 25 mM β-glycerolphosphate, and 1 × protease inhibitor cocktail, and the homogenates were centrifuged at 800 g for 10 min (4°C) to remove myofibrillar proteins. The protein concentration in each supernatant sample was determined with the DC protein assay Kit (Bio-Rad).

For western blotting, an equal amount of protein from each sample was boiled in Laemmli buffer, resolved on SDS-PAGE, transferred onto PVDF membrane (MilliporeSigma), blocked with 5% milk in PBS-T (PBS with 0.5% Tween 20), and probed with the indicated primary and secondary antibodies according to the manufacturers' recommendations. After washing in PBS-T, blots were developed and visualized using the SuperSignal West Pico PLUS Chemiluminescent Substrate and an iBright CL1000 Imaging System, respectively (both from Thermo Fisher Scientific). ImageJ (Schneider et al., 2012) was used to quantify each blot. The antibodies used in this study are as follows: anti-ARHGEF3 was previously reported (Khanna et al., 2013); anti-Myosin heavy chain type I (BA-D5), type IIA (SC-71), type IIX (6H1), type IIB (BF-F3), and sarcomere (MF 20) from Developmental Studies Hybridoma Bank; anti-COX IV (4844), Cytochrome c (4272), pSer473-Akt (9271), pThr308-Akt (9275), Akt (9272), pThr346-NDRG1 (3217), NDRG1 (9408), LC3A/B (4108), p62 (23214), RhoA (2117), and GAPDH (2118) from Cell Signaling Technology; anti-pSer657-PKCα (06-822) from MilliporeSigma; anti-PKCα (P4334) from Sigma-Aldrich; anti-F4/80 (MCA497G) from Bio-Rad; anti-c-*myc* (MMS-150R) from Covance; peroxidase-conjugated anti-rabbit (111-036-003), anti-mouse (115-036-003), anti-mouse light chain specific (115-035-174), and anti-rat (172-035-153) IgG antibodies from Jackson Immuno Research Laboratories.

RhoA GEF activity assay—Muscle homogenates were prepared in buffer A as described above and an equal amount of protein from each sample was incubated with 20 μL of Rhotekin-RBD beads (Cytoskeleton) for 2 hours at 4°C and washed 4 times in ice-cold buffer containing 50 mM Tris (pH 7.4), 1% Triton X-100, 150 mM NaCl, 10 mM $MgCl_2$, and 1 × protease inhibitor cocktail. The beads were boiled in Laemmli buffer and active form of GTP-bound RhoA was detected by western blotting with anti-RhoA primary antibody. RhoA-specific GEF activity was then determined by normalizing the amount of GTP-bound RhoA to the amount of total RhoA.

Quantitative PCR (qPCR)—Frozen muscles were homogenized with a Teflon-glass homogenizer in ice-cold TRIzol (Invitrogen), and total RNA was extracted using the RNeasy Mini Kit (QIAGEN) according to the manufacturer's instructions. The purity and integrity of RNA samples were confirmed by the ratio of A_{260}/A_{280} absorbance and of 28S/18S ribosomal RNA, respectively. cDNA was synthesized from 1 μg of RNA using the qScript cDNA Synthesis Kit (Quanta Bioscience) and subjected to qPCR on a StepOnePlus Real-Time PCR System (Applied Biosystems) using SYBR green. The primers used in this study are listed in Table S1

Quantification and Statistical Analysis—All values were presented as mean ± SEM unless otherwise noted, with individual animal data points shown in graphs (the number of the points represents n). Sample size for each experiment was determined on the basis of previous publications and preliminary data. Mice that showed any sign of abnormality according to pre-established criteria (e.g., lethargy, elevated respiration rate, reduced body weight, tumor, etc.) were excluded from experiments. A quantified sample value that deviated more than three times SD from the mean in a given group was considered as an outlier. Statistical significance ($p < 0.05$) was determined by two-tailed paired (when comparing to contralateral controls) or unpaired t tests for single comparisons or one- or two-way ANOVA followed by Student-Newman-Keuls post hoc test for multiple comparisons. All statistical analyses including assumption tests were performed using Excel or SigmaPlot 14.0.

Supplementary Material

Refer to Web version on PubMed Central for supplementary material.

ACKNOWLEDGMENTS

We thank Fuming Pan and the Transgenic Mouse Facility at the University of Illinois at Urbana-Champaign for pronuclear injection of TALEN mRNA and creation of founder transgenic mice. This work was supported by grants from the National Institutes of Health to J.C. (AR048914 and GM089771).

REFERENCES

Arthur WT, Ellerbroek SM, Der CJ, Burridge K, and Wennerberg K (2002). XPLN, a guanine nucleotide exchange factor for RhoA and RhoB, but not RhoC. J. Biol. Chem 277, 42964–42972. [PubMed: 12221096]

Berndt N, Yang H, Trinczek B, Betzi S, Zhang Z, Wu B, Lawrence NJ, Pellecchia M, Schönbrunn E, Cheng JQ, and Sebti SM (2010). The Akt activation inhibitor TCN-P inhibits Akt phosphorylation by binding to the PH domain of Akt and blocking its recruitment to the plasma membrane. Cell Death Differ. 17, 1795–1804. [PubMed: 20489726]

Brooks SV, and Faulkner JA (1988). Contractile properties of skeletal muscles from young, adult and aged mice. J. Physiol 404, 71–82. [PubMed: 3253447]

Bujak AL, Crane JD, Lally JS, Ford RJ, Kang SJ, Rebalka IA, Green AE, Kemp BE, Hawke TJ, Schertzer JD, and Steinberg GR (2015). AMPK activation of muscle autophagy prevents fasting-induced hypoglycemia and myopathy during aging. Cell Metab. 21, 883–890. [PubMed: 26039451]

Call JA, Wilson RJ, Laker RC, Zhang M, Kundu M, and Yan Z (2017). Ulk1-mediated autophagy plays an essential role in mitochondrial remodeling and functional regeneration of skeletal muscle. Am. J. Physiol. Cell Physiol 312, C724–C732. [PubMed: 28356270]

Carnio S, LoVerso F, Baraibar MA, Longa E, Khan MM, Maffei M, Reischl M, Canepari M, Loefler S, Kern H, et al. (2014). Autophagy impairment in muscle induces neuromuscular junction degeneration and precocious aging. Cell Rep. 8, 1509–1521. [PubMed: 25176656]

Celichowski J, and Grottel K (1993). Twitch/tetanus ratio and its relation to other properties of motor units. Neuroreport 5, 201–204. [PubMed: 8298075]

Charrasse S, Comunale F, Grumbach Y, Poulat F, Blangy A, and Gauthier-Rouvière C (2006). RhoA GTPase regulates M-cadherin activity and myoblast fusion. Mol. Biol. Cell 17, 749–759. [PubMed: 16291866]

Demontis F, and Perrimon N (2010). FOXO/4E-BP signaling in Drosophila muscles regulates organism-wide proteostasis during aging. Cell 143, 813–825. [PubMed: 21111239]

Fiacco E, Castagnetti F, Bianconi V, Madaro L, De Bardi M, Nazio F, D'Amico A, Bertini E, Cecconi F, Puri PL, and Latella L (2016). Autophagy regulates satellite cell ability to regenerate normal and dystrophic muscles. Cell Death Differ. 23, 1839–1849. [PubMed: 27447110]

Fling BW, Knight CA, and Kamen G (2009). Relationships between motor unit size and recruitment threshold in older adults: implications for size principle. Exp. Brain Res 197, 125–133. [PubMed: 19565231]

García-Martínez JM, and Alessi DR (2008). mTOR complex 2 (mTORC2) controls hydrophobic motif phosphorylation and activation of serum- and glucocorticoid-induced protein kinase 1 (SGK1). Biochem. J 416, 375–385. [PubMed: 18925875]

García-Prat L, Martínez-Vicente M, Perdiguero E, Ortet L, Rodríguez-Ubreva J, Rebollo E, Ruiz-Bonilla V, Gutarra S, Ballestar E, Serrano AL, et al. (2016). Autophagy maintains stemness by preventing senescence. Nature 529, 37–42. [PubMed: 26738589]

Goodpaster BH, Park SW, Harris TB, Kritchevsky SB, Nevitt M, Schwartz AV, Simonsick EM, Tylavsky FA, Visser M, and Newman AB (2006). The loss of skeletal muscle strength, mass, and quality in older adults: the health, aging and body composition study. J. Gerontol. A Biol. Sci. Med. Sci 61, 1059–1064. [PubMed: 17077199]

Hamrick MW, Ding KH, Pennington C, Chao YJ, Wu YD, Howard B, Immel D, Borlongan C, McNeil PL, Bollag WB, et al. (2006). Age-related loss of muscle mass and bone strength in mice is associated with a decline in physical activity and serum leptin. Bone 39, 845–853. [PubMed: 16750436]

Ikenoue T, Inoki K, Yang Q, Zhou X, and Guan KL (2008). Essential function of TORC2 in PKC and Akt turn motif phosphorylation, maturation and signalling. EMBO J. 27, 1919–1931. [PubMed: 18566587]

Iwasaki K, Hayashi K, Fujioka T, and Sobue K (2008). Rho/Rho-associated kinase signal regulates myogenic differentiation via myocardin-related transcription factor-A/Smad-dependent transcription of the Id3 gene. J. Biol. Chem 283, 21230–21241. [PubMed: 18477564]

Jiang BH, Aoki M, Zheng JZ, Li J, and Vogt PK (1999). Myogenic signaling of phosphatidylinositol 3-kinase requires the serine-threonine kinase Akt/protein kinase B. Proc. Natl. Acad. Sci. U S A 96, 2077–2081. [PubMed: 10051597]

Khanna N, Fang Y, Yoon MS, and Chen J (2013). XPLN is an endogenous inhibitor of mTORC2. Proc. Natl. Acad. Sci. U S A 110, 15979–15984. [PubMed: 24043828]

Kung TA, Cederna PS, van der Meulen JH, Urbanchek MG, Kuzon WM Jr., and Faulkner JA (2014). Motor unit changes seen with skeletal muscle sarcopenia in oldest old rats. J. Gerontol. A Biol. Sci. Med. Sci 69, 657–665. [PubMed: 24077596]

Le Grand F, and Rudnicki MA (2007). Skeletal muscle satellite cells and adult myogenesis. Curr. Opin. Cell Biol 19, 628–633. [PubMed: 17996437]

Lee DE, Bareja A, Bartlett DB, and White JP (2019). Autophagy as a therapeutic target to enhance aged muscle regeneration. Cells 8, 183. [PubMed: 30791569]

Levine B, and Kroemer G (2008). Autophagy in the pathogenesis of disease. Cell 132, 27–42. [PubMed: 18191218]

Lim MJ, Choi KJ, Ding Y, Kim JH, Kim BS, Kim YH, Lee J, Choe W, Kang I, Ha J, et al. (2007). RhoA/Rho kinase blocks muscle differentiation via serine phosphorylation of insulin receptor substrate-1 and -2. Mol. Endocrinol 21, 2282–2293. [PubMed: 17579208]

Mammucari C, Milan G, Romanello V, Masiero E, Rudolf R, Del Piccolo P, Burden SJ, Di Lisi R, Sandri C, Zhao J, et al. (2007). FoxO3 controls autophagy in skeletal muscle in vivo. Cell Metab. 6, 458–471. [PubMed: 18054315]

Metter EJ, Lynch N, Conwit R, Lindle R, Tobin J, and Hurley B (1999). Muscle quality and age: cross-sectional and longitudinal comparisons. J. Gerontol. A Biol. Sci. Med. Sci 54, B207–B218. [PubMed: 10362000]

Mleczak A, Millar S, Tooze SA, Olson MF, and Chan EY (2013). Regulation of autophagosome formation by Rho kinase. Cell. Signal 25, 1–11. [PubMed: 22975682]

Mu X, Usas A, Tang Y, Lu A, Wang B, Weiss K, and Huard J (2013). RhoA mediates defective stem cell function and heterotopic ossification in dystrophic muscle of mice. FASEB J. 27, 3619–3631. [PubMed: 23704088]

Panzhinskiy E, Culver B, Ren J, Bagchi D, and Nair S (2013). Role of mammalian target of rapamycin (mTOR) in muscle growth. In Nutrition and Enhanced Sports Performance: Muscle Building, Endurance, and Strength, Bagchi Debasis, Nair Sreejayan, and Sen Chandan K., eds. (New York: Elsevier), pp. 217–227.

Paolini A, Omairi S, Mitchell R, Vaughan D, Matsakas A, Vaiyapuri S, Ricketts T, Rubinsztein DC, and Patel K (2018). Attenuation of autophagy impacts on muscle fibre development, starvation induced stress and fibre regeneration following acute injury. Sci. Rep 8, 9062. [PubMed: 29899362]

Rossman KL, Der CJ, and Sondek J (2005). GEF means go: turning on RHO GTPases with guanine nucleotide-exchange factors. Nat. Rev. Mol. Cell Biol 6, 167–180. [PubMed: 15688002]

Russ DW, Gregg-Cornell K, Conaway MJ, and Clark BC (2012). Evolving concepts on the age-related changes in “muscle quality.”. J. Cachexia Sarcopenia Muscle 3, 95–109. [PubMed: 22476917]

Schneider CA, Rasband WS, and Eliceiri KW (2012). NIH Image to ImageJ: 25 years of image analysis. Nat. Methods 9, 671–675. [PubMed: 22930834]

Sebastián D, Sorianello E, Segalés J, Irazoki A, Ruiz-Bonilla V, Sala D, Planet E, Berenguer-Llergo A, Muñoz JP, Sánchez-Feutrie M, et al. (2016). Mfn2 deficiency links age-related sarcopenia and impaired autophagy to activation of an adaptive mitophagy pathway. EMBO J. 35, 1677–1693. [PubMed: 27334614]

Shi J, Surma M, and Wei L (2018). Disruption of ROCK1 gene restores autophagic flux and mitigates doxorubicin-induced cardiotoxicity. Oncotarget 9, 12995–13008. [PubMed: 29560126]

Shi J, Surma M, Yang Y, and Wei L (2019). Disruption of both ROCK1 and ROCK2 genes in cardiomyocytes promotes autophagy and reduces cardiac fibrosis during aging. FASEB J. 33, 7348–7362. [PubMed: 30848941]

Sun N, and Zhao H (2013). Transcription activator-like effector nucleases (TALENs): a highly efficient and versatile tool for genome editing. Biotechnol. Bioeng 110, 1811–1821. [PubMed: 23508559]

Takano H, Komuro I, Oka T, Shiojima I, Hiroi Y, Mizuno T, and Yazaki Y (1998). The Rho family G proteins play a critical role in muscle differentiation. Mol. Cell. Biol 18, 1580–1589. [PubMed: 9488475]

Thorburn A (2018). Autophagy and disease. J. Biol. Chem 293, 5425–5430. [PubMed: 29191833]

Tidball JG (2017). Regulation of muscle growth and regeneration by the immune system. Nat. Rev. Immunol 17, 165–178. [PubMed: 28163303]

Tidball JG, and Villalta SA (2010). Regulatory interactions between muscle and the immune system during muscle regeneration. Am. J. Physiol. Regul. Integr. Comp. Physiol 298, R1173–R1187. [PubMed: 20219869]

Wang RC, Wei Y, An Z, Zou Z, Xiao G, Bhagat G, White M, Reichelt J, and Levine B (2012). Akt-mediated regulation of autophagy and tumorigenesis through Beclin 1 phosphorylation. Science 338, 956–959. [PubMed: 23112296]

Wei L, Zhou W, Croissant JD, Johansen FE, Prywes R, Balasubramanyam A, and Schwartz RJ (1998). RhoA signaling via serum response factor plays an obligatory role in myogenic differentiation. J. Biol. Chem 273, 30287–30294. [PubMed: 9804789]

Yang L, Dan HC, Sun M, Liu Q, Sun XM, Feldman RI, Hamilton AD, Polokoff M, Nicosia SV, Herlyn M, et al. (2004). Akt/protein kinase B signaling inhibitor-2, a selective small molecule inhibitor of Akt signaling with antitumor activity in cancer cells overexpressing Akt. Cancer Res. 64, 4394–4399. [PubMed: 15231645]

You JS, Dooley MS, Kim CR, Kim EJ, Xu W, Goodman CA, and Hornberger TA (2018). A DGKζ-FoxO-ubiquitin proteolytic axis controls fiber size during skeletal muscle remodeling. Sci. Signal 11, eaao6847. [PubMed: 29764991]

Highlights

- Depletion of ARHGEF3 in mice enhances injury-induced skeletal muscle regeneration
- ARHGEF3 function in regeneration depends on its GEF activity and not Akt
- RhoA/ROCK and autophagy mediate ARHGEF3-regulated muscle regeneration
- By restoring autophagy, ARHGEF3 deficiency prevents age-related muscle weakness

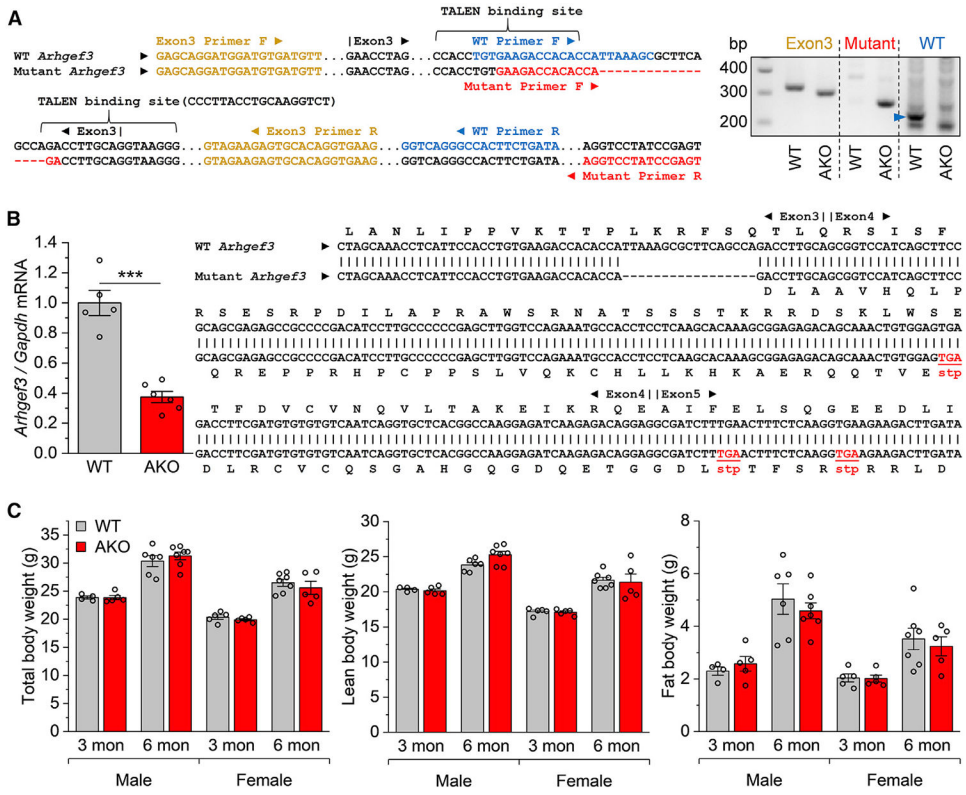

Figure 1. Generation of ARHGEF3-KO Mice

(A) Genomic DNA extracted from TA muscles of WT and ARHGEF3-KO (AKO) mice was PCR-amplified with three different primer sets (left panel), and the amplicons were detected using agarose gel electrophoresis (right panel). The sizes of amplicons are 322 bp (exon 3, WT), 305 bp (exon 3, AKO), 261 bp (mutant), and 241 bp (WT).

(B) cDNA from mRNA extracted from TA muscles of WT and AKO mice was subjected to quantitative PCR analysis (left panel; n = 5 or 6) or sequenced (right panel).

(C) Body compositions were analyzed in 3- and 6-month-old WT and AKO mice (n = 4–7). Data are presented as mean ± SEM. ***p < 0.001 by two-tailed unpaired t test. See also Figure S1.

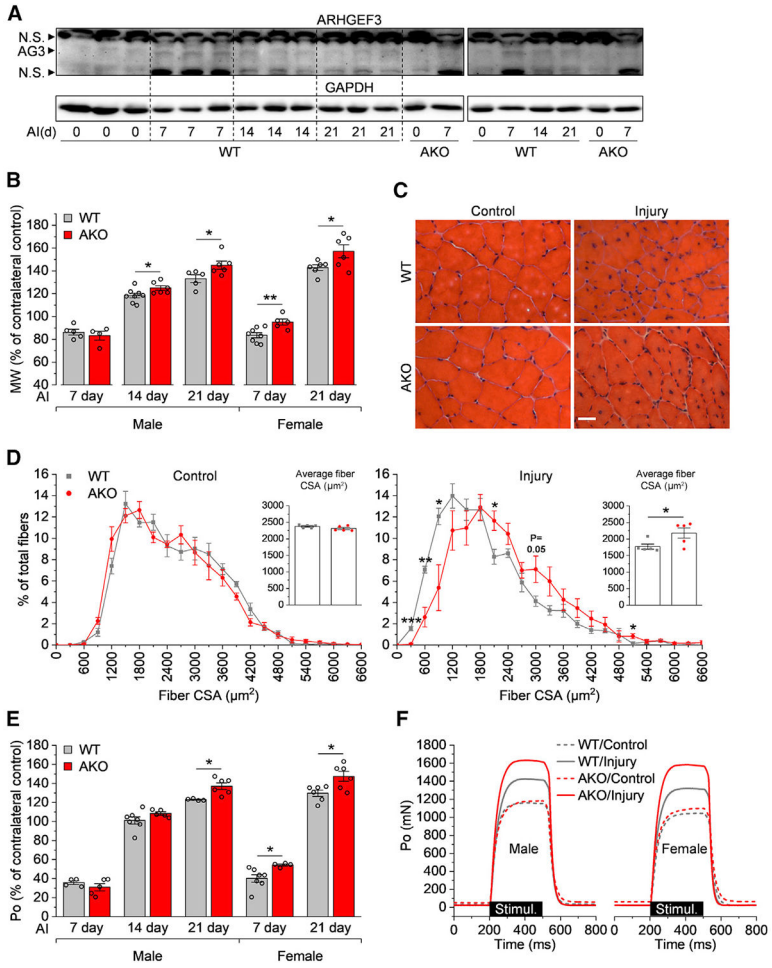

Figure 2. ARHGEF3 KO Promotes Skeletal Muscle Regeneration after Injury

TA muscles from 3-month-old WT and ARHGEF3-KO (AKO) mice were injected with $BaCl_2$ (injury) or saline (uninjured control, day 0).

(A) Protein expression of ARHGEF3 (AG3) and GAPDH was analyzed using western blotting in female muscles collected 7, 14, and 21 days after injury (AI) (n = 4 in WT). N.S., non-specific.

(B) Muscle weight (MW) was measured 7, 14, and 21 days after AI and presented as percentage of contralateral uninjured control (n = 4–8).

(C) Representative H&E images of cross sections of injured and uninjured muscles collected 21 days AI from male mice. Scale bar: 50 μm.

(D) Cross-sectional area (CSA) of myofibers was measured from the H&E images and presented on histograms with inserts showing averaged CSA (n = 5).

(E) Maximal isometric tetanic force (Po) was measured 7, 14, and 21 days AI and presented as percentage of contralateral uninjured control (n = 4–7). Note that at 14 d AI, only the Po of AKO muscles was significantly higher than uninjured contralateral controls.

(F) Representative trace of maximal isometric tetanic force during stimulation (300 ms) at 21 days AI.

Data are presented as mean ± SEM. *p < 0.05 and **p < 0.01 by two-tailed unpaired t test unless otherwise indicated.

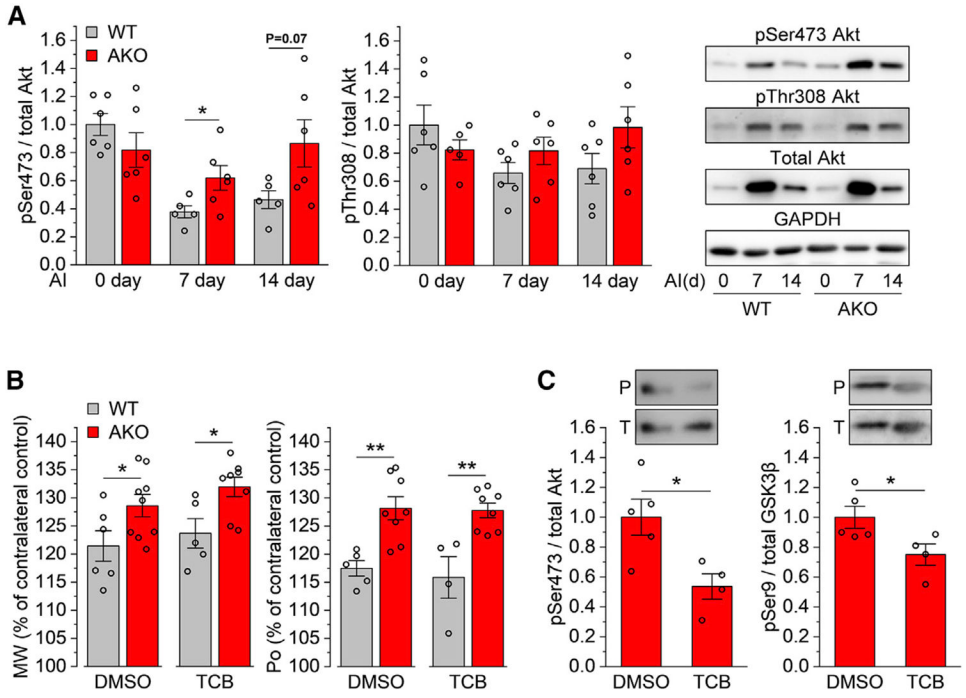

Figure 3. ARHGEF3 Regulation of Muscle Regeneration Is Independent of Its Effect on Akt Signaling

TA muscles from 3-month-old WT and ARHGEF3-KO (AKO) male mice were injected with $BaCl_2$ (injury) or saline (uninjured control, day 0).

(A) The muscles were collected 7 and 14 days after injury (AI) and analyzed using western blotting for phosphorylated/total Akt ratio and GAPDH protein expression (n = 5 or 6).

(B and C) Mice were treated with vehicle (DMSO) or triciribine (TCB) upon injury. Muscle weight (MW) and maximal isometric tetanic force (Po) were measured 21 days AI and presented as percentage of contralateral uninjured control (B) (n = 4–9). Phosphorylated (P)/total (T) protein ratio for Akt and GSK3β was determined using western blotting in injured AKO muscles collected 21 days AI (C) (n = 4 or 5).

Data are presented as mean ± SEM. *p < 0.05 and **p < 0.01 by two-tailed unpaired t test (A and C) or two-way ANOVA (B). See also Figure S2.

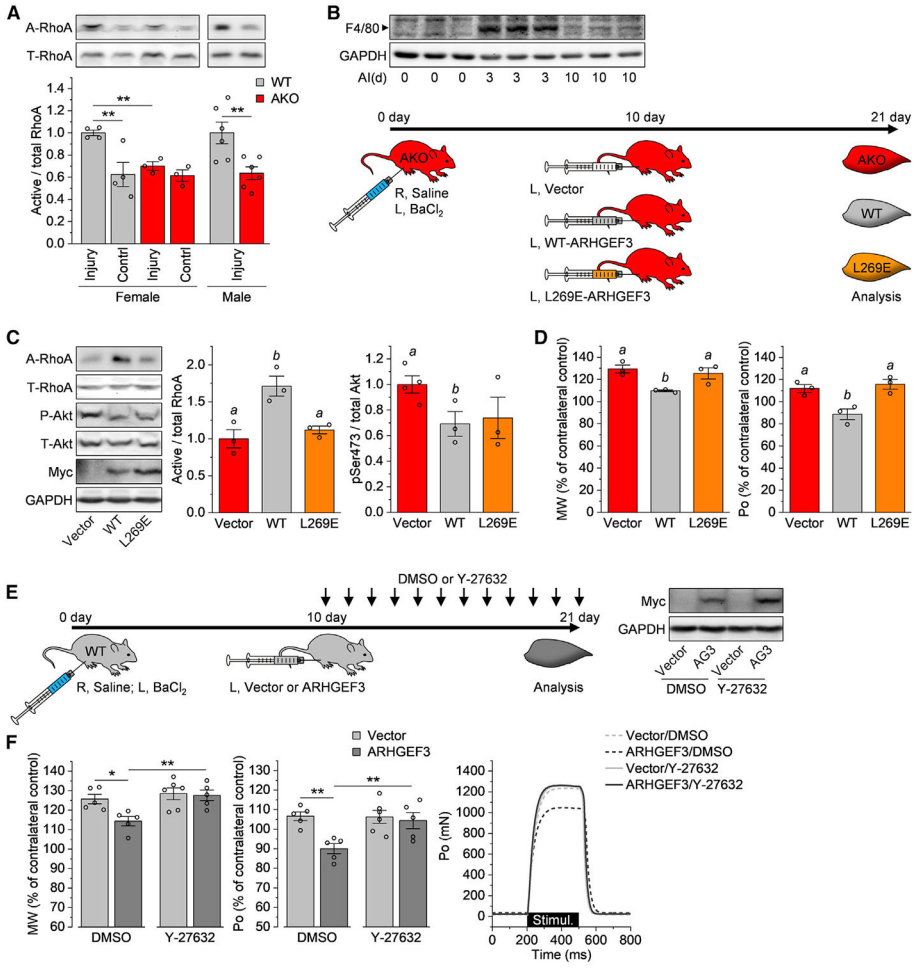

Figure 4. The GEF Activity of ARHGEF3 toward ROCK Is Critical for the Regulation of Muscle Regeneration

(A) TA muscles from 3-month-old WT and ARHGEF3-KO (AKO) mice were injected with $BaCl_2$ (injury) or saline (uninjured control), collected 14 days after injury, and analyzed using western blotting for active (A)/total (T) RhoA ratio (n = 3–6).

(B) TA muscles from AKO male mice were injected with $BaCl_2$ (injury) or saline (uninjured control; day 0) and either collected 3 and 10 days (d) after injury (AI) for analysis of F4/80 and GAPDH protein expression using western blotting (upper panel; n = 3) or transfected with empty vector, Myc-ARHGEF3 (WT), or Myc-ARHGEF3-L269E 10 days AI and allowed to recover until 21 days AI (lower panel).

(C) The transfected injured muscles in (B) were analyzed using western blotting for active (A)/total (T) RhoA ratio, phosphorylated (P)/total Akt ratio, and Myc-tagged ARHGEF3 and GAPDH protein expression (n = 3).

(D) The muscles in (B) were analyzed for muscle weight (MW) and maximal isometric tetanic force (Po), and the values were presented as percentage of contralateral uninjured control (n = 3).

(E) TA muscles from WT male mice were injured and transfected with empty vector or Myc-ARHGEF3 (AG3) as in (B) and treated with vehicle (DMSO) or Y-27632 upon

transfection. Right panel shows expression of Myc-tagged ARHGEF3 protein analyzed using western blotting.

(F) The muscles in (E) were analyzed for muscle weight (MW) and maximal isometric tetanic force (Po), and the values were presented as percentage of contralateral uninjured control (n = 5 or 6).

Data are presented as mean ± SEM. *p < 0.05 and **p < 0.01 by two-way ANOVA or two-tailed unpaired t test (A, male); *a* and *b* differ from each other at p < 0.05 by one-way ANOVA or two-tailed unpaired t test (C, Akt). See also Figure S3.

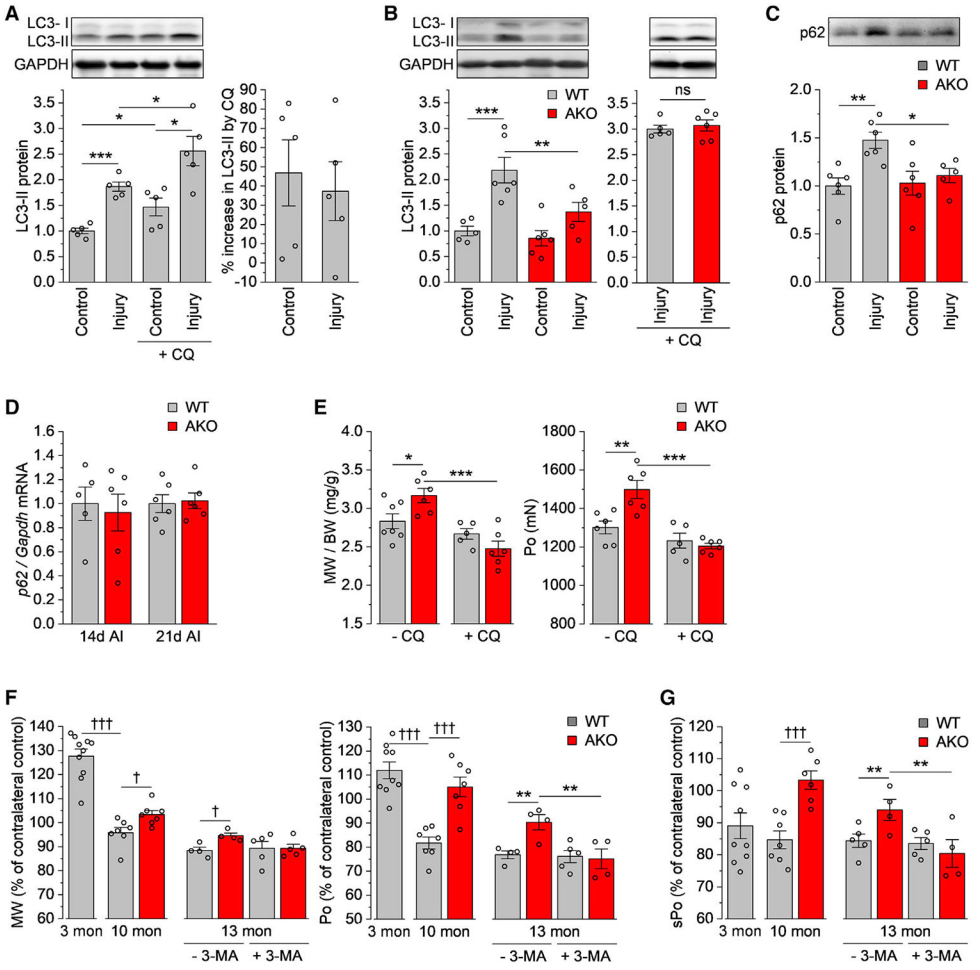

Figure 5. ARHGEF3 KO Promotes Muscle Regeneration through Autophagy and Prevents Age-Related Regenerative Defects

TA muscles from WT and/or ARHGEF3-KO (AKO) female mice were injected with $BaCl_2$ (injury) or saline (uninjured control) and allowed to recover with or without the indicated drug treatment. CQ, chloroquine; 3-MA, 3-methyladenine.

(A) Protein expression of LC3-II and GAPDH was analyzed using western blotting in 3-month-old WT muscles collected 21 days after injury (n = 5).

(B and C) Protein expression of LC3-II, GAPDH (B), and p62 (C) was analyzed using western blotting in 3-month-old WT and AKO muscles collected 21 days after injury (n = 5 or 6).

(D) mRNA expression of *p62* was analyzed using qPCR in 3-month-old WT and AKO muscles collected 14 and 21 days after injury (AI) (n = 5 or 6).

(E) Muscle weight (MW)/body weight (BW) ratio and maximal isometric tetanic force (Po) were measured in 3-month-old WT and AKO injured muscles 21 days after injury (n = 5–7).

(F and G) Muscle weight (MW), maximal isometric tetanic force (Po) (F), and specific maximal isometric tetanic force (sPo) (G) were measured in 3-, 10-, and/or 13-month-old WT and AKO muscles 14 days after injury and presented as percentage of contralateral uninjured control (n = 4–10).

Data are presented as mean ± SEM. *p < 0.05, **p < 0.01, and ***p < 0.001 by two-way ANOVA; $^{\dagger}p < 0.05$ and $^{\dagger\dagger}p < 0.01$ by two-tailed unpaired t test. See also Figure S4.

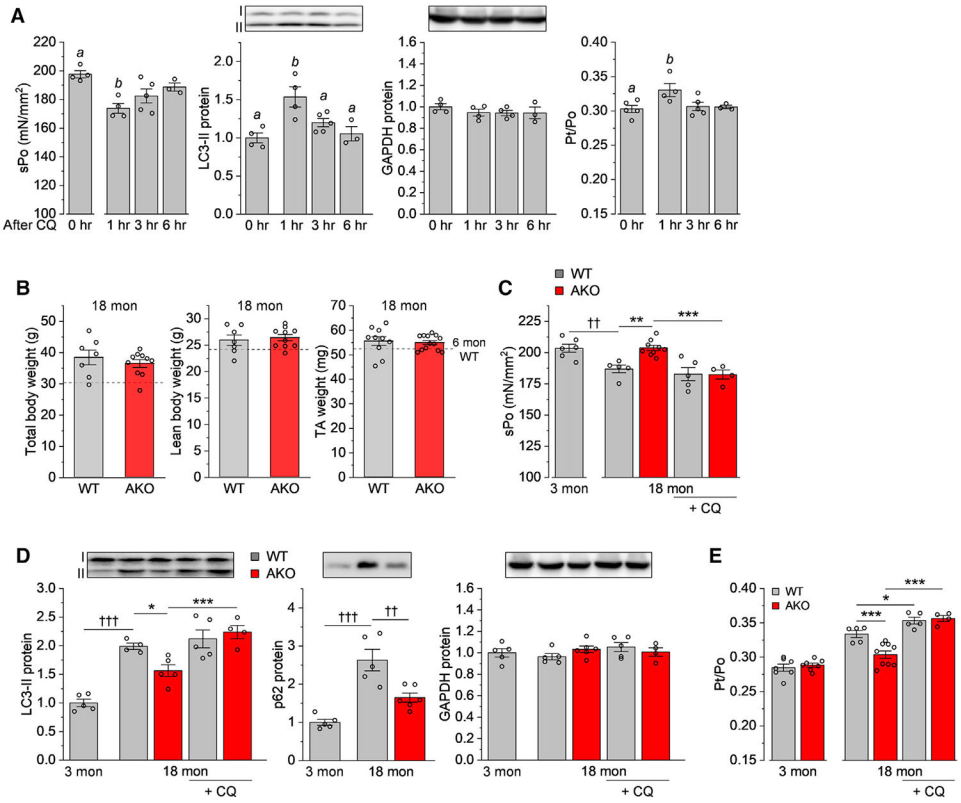

Figure 6. ARHGEF3 KO Prevents Age-Related Muscle Weakness by Restoring Autophagy

(A) Three-month-old mice were injected with vehicle (0 h) or chloroquine (CQ), and at indicated time points, TA muscles were analyzed for specific maximal isometric tetanic force (sPo) and collected for analysis of LC3-II and GAPDH protein expression using western blotting (n = 3–5). The muscles were also analyzed for maximal twitch force (Pt)/maximal tatanic force (Po) ratio (n = 3–5).

(B) Eighteen-month-old WT and ARHGEF3-KO (AKO) male mice were analyzed for total body weight, lean body weight, and TA muscle weight (n = 7–13). Dashed lines represent mean values from 6-month-old WT male mice (n = 6 or 7).

(C–E) Three- and/or 18-month-old WT and AKO male mice were injected with vehicle or CQ, and at 1 h after the injection, TA muscles were analyzed for sPo (C) (n = 4–9) and collected for analysis of LC3-II, p62, and GAPDH protein expression using western blotting (D) (n = 4–6). The muscles were also analyzed for Pt/Po ratio (E) (n = 4–9).

Data are presented as mean ± SEM. *a* and *b* differ from each other at $p < 0.05$ by 1-way ANOVA; $^{\dagger\dagger}p < 0.01$ and $^{\dagger\dagger\dagger}p < 0.001$ by 2-tailed unpaired t test; $^{*}p < 0.05$, $^{**}p < 0.01$, and $^{***}p < 0.001$ by two-way ANOVA.

KEY RESOURCES TABLE

REAGENT or RESOURCE	SOURCE	IDENTIFIER
Antibodies		
Rabbit polyclonal anti-ARHGEF3	Jie Chen lab (University of Illinois at Urbana-Champaign); Khanna et al., 2013	N/A
Mouse monoclonal anti-Myosin heavy chain Type I	Developmental Studies Hybridoma Bank	Cat#BA-D5; RRID: AB_2235587
Mouse monoclonal anti-Myosin heavy chain Type IIA	Developmental Studies Hybridoma Bank	Cat#SC-71; RRID: AB_2147165
Mouse monoclonal anti-Myosin heavy chain Type IIX	Developmental Studies Hybridoma Bank	Cat#6H1; RRID: AB_1157897
Mouse monoclonal anti-Myosin heavy chain Type IIB	Developmental Studies Hybridoma Bank	Cat#BF-F3; RRID: AB_2266724
Mouse monoclonal anti-Myosin heavy chain, sarcomere	Developmental Studies Hybridoma Bank	Cat#MF 20; RRID: AB_2147781
Rabbit polyclonal anti-COX IV	Cell Signaling Technology	Cat#4844; RRID: AB_2085427
Rabbit polyclonal anti-Cytochrome c	Cell Signaling Technology	Cat#4272; RRID: AB_209045
Rabbit polyclonal anti-pSer473-Akt	Cell Signaling Technology	Cat#9271; RRID: AB_329825
Rabbit polyclonal anti-pThr308-Akt	Cell Signaling Technology	Cat#9275; RRID: AB_329828
Rabbit polyclonal anti-Akt	Cell Signaling Technology	Cat#9272; RRID: AB_329827
Rabbit polyclonal anti-pThr346-NDRG1	Cell Signaling Technology	Cat#3217; RRID: AB_2150174
Rabbit monoclonal anti-NDRG1	Cell Signaling Technology	Cat#9408; Clone D6C2; RRID: AB_11140640
Rabbit polyclonal anti-LC3A/B	Cell Signaling Technology	Cat#4108; RRID: AB_2137703
Rabbit monoclonal anti-SQSTM1/p62	Cell Signaling Technology	Cat#23214; Clone D6M5X; RRID: AB_2798858
Rabbit monoclonal anti-RhoA	Cell Signaling Technology	Cat#2117; Clone 67B9; RRID: AB_10693922
Rabbit monoclonal anti-GAPDH	Cell Signaling Technology	Cat#2118; Clone 14C10; RRID: AB_561053
Rabbit polyclonal anti-pSer657-PKCα	MilliporeSigma	Cat#06-822; RRID: AB_310258
Rabbit polyclonal anti-PKCα	Sigma-Aldrich	Cat#P4334; RRID: AB_477345
Rat monoclonal anti-F4/80	Bio-Rad	Cat#MCA497G; Clone CI:A3-1; RRID: AB_872005
Rabbit polyclonal anti-c-myc	Covance	Cat#MMS-150R-1000, Clone 9E10; RRID: AB_291325
Chemicals, Peptides, and Recombinant Proteins		
Barium chloride ($BaCl_2$)	Sigma-Aldrich	Cat#202738; CAS: 10361-37-2
Triciribine	MilliporeSigma	Cat#124012; CAS: 35943-35-2
Y-27632 dihydrochloride	Tocris Bioscience	Cat#1254; CAS: 129830-38-2
Chloroquine diphosphate salt	Sigma-Aldrich	Cat#C6624; CAS: 50-63-5
3-Methyladenine	Sigma-Aldrich	Cat#M9281; CAS: 5142-23-4
Rhotekin-RBD beads	Cytoskeleton	Cat#RT02
Experimental Models: Organisms/Strains		
Mouse: C57BL/6N; ARHGEF3$^{-/-}$	This paper	N/A
Oligonucleotides		
See Figure 1A for genotyping primers	Integrated DNA Technologies	N/A
See Table S1 for qPCR primers	Integrated DNA Technologies	N/A

REAGENT or RESOURCE	SOURCE	IDENTIFIER
Recombinant DNA		
Plasmid: pcDNA3	Jie Chen lab (University of Illinois at Urbana-Champaign)	N/A
Plasmid: pCMV-Myc-ARHGEF3 (XPLN)	Arthur et al., 2002	Addgene Plasmid #73365
Plasmid: pCMV-Myc-ARHGEF3 (XPLN)-L269E	Khanna et al., 2013	Addgene Plasmid #73376
Software and Algorithms		
ImageJ	Schneider et al., 2012	https://imagej.nih.gov/ij/
SigmaPlot 14.0	Systat Software	https://systatsoftware.com/
Other		
1300A: 3-in-1 Whole Animal System	Aurora Scientific	N/A
iBright CL1000 Imaging System	ThermoFisher Scientific	N/A